Binary matrices of optimal autocorrelations as alignment marks

Scott A. Skirlo,[a] Ling Lu,[b] and Marin Soljačić
Department of Physics, Massachusetts Institute of Technology, Cambridge, Massachusetts 02139

(Received 4 November 2014; accepted 6 February 2015; published 23 February 2015)

The authors define a new class of binary matrices by maximizing the peak-sidelobe distances in the aperiodic autocorrelations. These matrices can be used as robust position marks for in-plane translational spatial alignment. The optimal square matrices of dimensions up to 7×7 and optimal diagonally symmetric matrices of 8×8 and 9×9 were found by exhaustive searches. © *2015 American Vacuum Society*. [http://dx.doi.org/10.1116/1.4913316]

I. INTRODUCTION

Binary sequences[1,2] and matrices with good autocorrelation properties have key applications in digital communications (radar, sonar, CDMA, and cryptography)[3] and in coded aperture imaging.[4] Several works have conducted exhaustive searches for the optimal matrices of these applications.[5–8] A less developed application of binary matrices with good aperiodic autocorrelations is two-dimensional (2D) translational spatial alignment. For example, it has been shown in electron-beam lithography[9–12] that position marks based on such binary matrices are immune to noise and manufacturing errors. However, the symbols that were used in these prior works were borrowed from different applications, noticeably the 1D Barker sequences from communications. There have been no studies on the optimal patterns for translational alignment.

In this paper, we define and report the optimal binary matrices as alignment marks. Section II sets up the problem. Section III defines the criteria for the optimal matrices. Section IV discusses previous work related to this problem. Section V works out the useful bounds. Section VI explains the exhaustive computer searches and lists the results. Section VII discusses several key observations of the optimal marks. Section VIII compares the performance of optimal and nonoptimal marks through simulations. Section IX discusses the potential applications of the matrices found. Section X concludes the paper.

II. PRELIMINARIES

An alignment mark is made by creating a surface pattern different from the background so that the pattern information transforms into a two-level signal when a digital image is taken. This image can be represented as a binary matrix where 1 represents the (black) pattern pixels and 0 represents the (white) background pixels or vice versa.

The 2D aperiodic autocorrelation (A) of an M by N binary matrix with elements $R_{i,j}$ is defined as

$$A(\tau_1, \tau_2) = \sum_{i=1}^{M} \sum_{j=1}^{N} R_{i,j} R_{i+\tau_1, j+\tau_2}, \tag{1}$$

where τ_1 and τ_2 are integer shifts. The peak value is $A(0, 0)$ while all other values are sidelobes. A is an inversion-symmetric $[A(\tau_1, \tau_2) = A(-\tau_1, -\tau_2)]$ $(2M-1) \times (2N-1)$ matrix. The crosscorrelation between R and the data image matrix $D_{i,j}$ is expressed as

$$C(\tau_1, \tau_2) = \sum_{i=1}^{M} \sum_{j=1}^{N} R_{i,j} D_{i+\tau_1, j+\tau_2}. \tag{2}$$

When the data D is a noisy version of the reference R, the peak value of the crosscorrelation determines the most probable position of the mark.

It is important to note that all the matrices are implicitly padded with 0s for all the matrix elements of indices exceeding their matrix dimensions.

A linear transformation of the data matrix results in a linear transformation of the correlation as long as the reference matrix is kept the same. This can be seen from

$$D'_{i,j} = cD_{i,j} + d, \tag{3}$$

$$C'(\tau_1, \tau_2) = cC(\tau_1, \tau_2) + d \sum_{i=1}^{M} \sum_{j=1}^{N} R_{i,j}, \tag{4}$$

where the second term of C' is a constant. The data matrix can thus be arbitrarily scaled ($c \neq 0$) while keeping the correlation equivalent and the alignment results identical.

III. CRITERIA FOR THE OPTIMAL BINARY MATRICES

Depending on the quantities being optimized, the criteria for the optimal matrices are different. For alignment purposes, we list two criteria here. The first is to minimize the misalignment probability. The second is to minimize the misalignment deviation. The first criterion depends on the values of the autocorrelation sidelobes, while the second one depends on their positions relative to the central peak.

In this paper, we chose to minimize the probability that misalignment happens. A misalignment occurs when one of the sidelobes exceeds the central peak $[p = A(0,0)]$; this probability is analytically expressed in Appendix A. Under the same noise condition, the less the peak-sidelobe distance the higher the misalignment probability. Consequently, the criteria for ranking the matrices are based on their peak-sidelobe distances.

[a]Electronic mail: sskirlo@mit.edu
[b]Electronic mail: linglu@mit.edu

The peak-sidelobe distances are illustrated in Fig. 1. We plotted an autocorrelation matrix $A(\tau)$ with peak value p and highest sidelobe value s. The shortest peak-sidelobe distance is denoted as d_1, where $d_1 = p - s$. The other distances are defined as $d_{i+1} = d_i + 1$ for $i \geq 1$, as shown for d_1 through d_4 in Fig. 1. n_i gives the number of times d_i occurs in the autocorrelation and $\sum_i n_i = (2M-1)(2N-1) - 1$. The histogram of an autocorrelation matrix can be expressed as $\{d_1 | n_1, n_2, ..., n_{(s+1)}\}$.

The criteria for finding the optimal matrix are to maximize d_1 and then minimize n_i sequentially in the dictionary order. These criteria are completely justified in the low noise limit in Appendix A, although a general criteria depends on the amount of noise in the data matrices. *Matrices of any size* can be compared using these criteria. In general, the distances (d_i) of the autocorrelation increase with the size of the matrix. Without restricting the matrix dimension, the optimal matrix will diverge in size. Consequently, we study the optimal matrix for each *fixed dimension*. Interestingly, the optimal matrices found in this paper are unique as discussed in Sec. VII.

IV. RELATED WORK

Previous works on 1 and −1 matrices with 0 background[5,8] in digital communications are different than our work on 1 and 0 matrices. The former representation has three levels (1,−1,0) while our binary matrices have only two levels. The aperiodic autocorrelations of these matrices are not equivalent.

Other works on binary matrices of 1s and 0s with aperiodic autocorrelations have used different criteria selected for applications in radar and sonar. In the Costas-array problem,[6] only one black pixel is placed per column and row and the maximum sidelobe is fixed to one. In the Golomb-rectangle problem,[7] the number of black pixels is maximized with the restriction that the sidelobe still be fixed to one.[13] However, our criteria does bear some resemblance to those in some of the works on one dimensional −1 and 1 (three levels) sequences.[2]

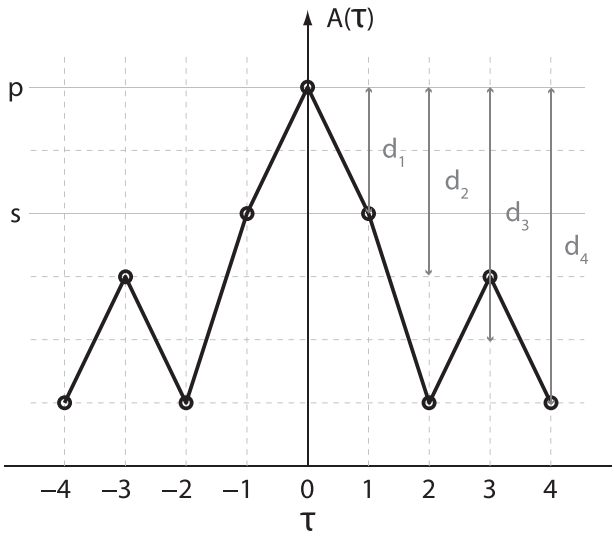

FIG. 1. We illustrate an autocorrelation function $A(\tau)$, whose peak value is p, highest sidelobe value is s, and whose peak-sidelobe distances are d_i.

V. TWO UPPER BOUNDS OF $d_{1,\max}(p)$, $d_{1,\max}^{\text{upper,I}}(p)$ AND $d_{1,\max}^{\text{upper,II}}(p)$

For a binary matrix R, the peak value p of its autocorrelation A equals the number of ones in the matrix (R). The largest d_1 for all matrices with a given p, of a fixed dimension, is $d_{1,\max}(p)$. $d_{1,\max}(p) = p - s_{\min}(p)$, where $s_{\min}(p)$ is the minimum highest sidelobe value as a function of p.

In this section, we constructed an upperbound of $d_{1,\max}(p)$, $d_{1,\max}^{\text{upper,I}}(p)$, by maximizing $p - A(\pm 1, 0)$. The $A(\pm 1, 0)$ computed here forms a lower bound on $s_{\min}(p)$, $s_{\min}^{\text{lower,I}}(p)$. This construction is illustrated in Fig. 2, where we assume the matrix R used to construct our bound is of dimension $M \times N$ with $M \leq N$.

We find:

$$d_{1,\max}^{\text{upper,I}}(p) = \begin{cases} p, & p \in [0, N_1] \quad \text{I} \\ N_1, & p \in [N_1, N_2] \quad \text{II} \\ M(N+1) - p, & p \in [N_2, MN] \quad \text{III} \end{cases}, \tag{5}$$

where $N_1 = MN/2, N_2 = (MN/2) + M$ when MN is even and $N_1 = (MN+1)/2, N_2 = [(MN+1)/2] + (M-1)$ when MN is odd.

This upper bound can be derived by starting out with a matrix $R_{i,j} = 0$ for all (i, j) and "filling in" with ones in a particular pattern. In region I, ones can be placed anywhere in $R_{i,j}$ where $i + j$ is odd. When $p = N_1$, we have formed a "checkerboard pattern." In region II, we place ones wherever $i + j$ is even for $i = 1$ or $i = N$. In region III, the remaining locations without ones are filled.

The autocorrelation function $A(\tau_1, \tau_2)$ equals the number of black squares that are connected by a displacement vector (τ_1, τ_2). We can use this property to construct a second lower

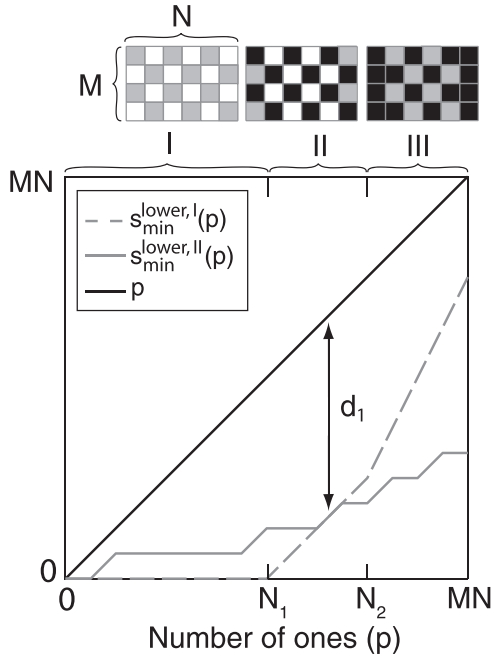

FIG. 2. Lowerbounds of $s_{\min}(p)$, $s_{\min}^{\text{lower,I}}(p)$ and $s_{\min}^{\text{lower,II}}(p)$. p is the autocorrelation peak. The three matrices on top illustrate the methods of filling black pixels for regions I, II, and III for the matrix construction of $s_{\min}^{\text{lower,I}}(p)$. The gray pixels show spots to be filled in that region, while the black pixels are spots that have been filled in previous regions.

bound $s_{\min}^{\text{lower,II}}(p)$. This approach is similar to the method used in Ref. 13.

Since the autocorrelation is invariant under inversion, there are $[(2M-1)(2N-1)-1]/2 = 2NM - N - M$ unique nonzero displacements; a matrix of p ones fills $p(p-1)/2$ of them. As p increases, there are repeated displacements because $p(p-1)/2$ quickly exceeds $2NM - N - M$.

We can find a lowerbound $s_{\min}^{\text{lower,II}}(p)$ by assuming that the displacements added to the autocorrelation function distribute uniformly, that is $|A(\tau_1,\tau_2) - A(\tau_2',\tau_2')| \leq 1$ for nonzero displacements. This gives $s_{\min}^{\text{lower,II}}(p) = ceil([p(p-1)]/[4NM - 2N - 2M])$, where $ceil[x]$ rounds to the nearest integer greater than x. Consequently, $d_{1,\max}^{\text{upper,II}} = p - ceil([p(p-1)]/[4NM - 2N - 2M])$.

As illustrated in Fig. 2, $s_{\min}^{\text{lower,II}}(p)$ is a better bound for small p, while $s_{\min}^{\text{lower,I}}(p)$ is a better bound for large p. The first bound $s_{\min}^{\text{lower,I}}(p)$, which keeps track of the pixel positions, becomes exact when p approaches "MN" (filled). While the second bound $s_{\min}^{\text{lower,II}}(p)$, which ignores the actual pixel locations, becomes exact when the matrix is sparse and p approaches "0" (empty).

VI. EXHAUSTIVE COMPUTER SEARCHES FOR THE OPTIMAL SQUARE MATRICES

Physical in-plane alignment usually requires equal alignment accuracies in both directions; this calls for square matrices ($M=N$). We applied exhaustive searches to find the square matrices with the maximum $d_1(=\max[d_{1,\max}(p)])$. The resulting matrices were ranked using the criteria in Sec. III to obtain the optimal matrices.

Backtrack conditions based on symmetries and sidelobes have been found useful in exhaustive searches for binary matrices.[5,13,14] Matrices related by symmetry operations are considered the same matrix. The symmetry operations for square matrices are horizontal and vertical flips and rotations by multiples of 90°. For this study, a backtrack condition based on eliminating redundant matrices related by horizontal flips was implemented. Backtrack conditions based on sidelobe levels are useful if the sidelobes are being minimized. However, we are maximizing the peak-sidelobe distance d_1, so the sidelobe backtrack condition was not used.

The search algorithm we implemented works by exhaustively generating matrices row by row. The algorithm continues generating rows until a backtrack condition occurs, or a matrix is completely specified. The matrix is stored for later ranking if it has the same or greater d_1 than the existing maximum d_1.

Several techniques were implemented to speed up the algorithm. Each matrix row was represented as a binary word so that fast bit-wise operations could be used. In addition lookup tables were created to calculate the horizontal flips and correlations of rows. For our binary matrices, the maximum sidelobes were typically located near the autocorrelation peak. Because of this, the sidelobe values were checked in a spiral pattern around the peak to quickly determine if a matrix had a d_1 less than the stored maximum.

The search results for square matrices of size up to 7×7 are presented in Fig. 3. Figure 3(a) gives the optimal

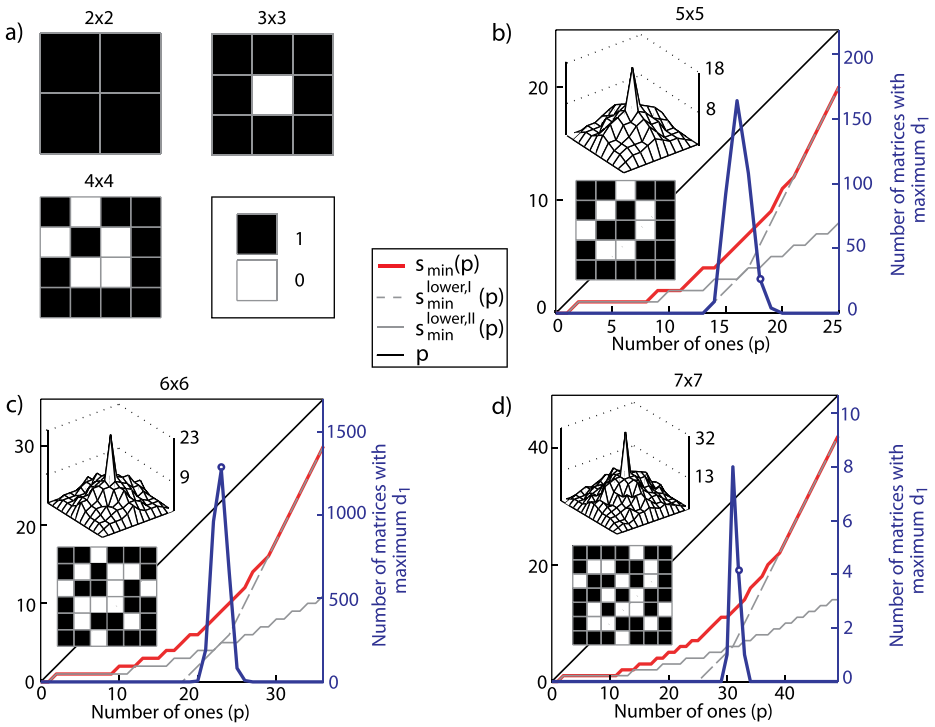

FIG. 3. (Color online) Results of the exhaustive searches for 2×2 to 7×7 matrices. (a) The optimal matrices from 2×2 to 4×4 are shown. (b)–(d) $s_{\min}(p)$ is the first line below the diagonal line. The first solid gray line bounding $s_{\min}(p)$ from below is $s_{\min}^{\text{lower,I}}(p)$, while the second dotted gray line bounding $s_{\min}(p)$ from below is $s_{\min}^{\text{lower,II}}(p)$. The number of matrices having the maximum d_1 is the peaked line. The circle specifies the location of the optimal matrix. The optimal matrices are presented as insets below their autocorrelations, which are labeled with their p and s values.

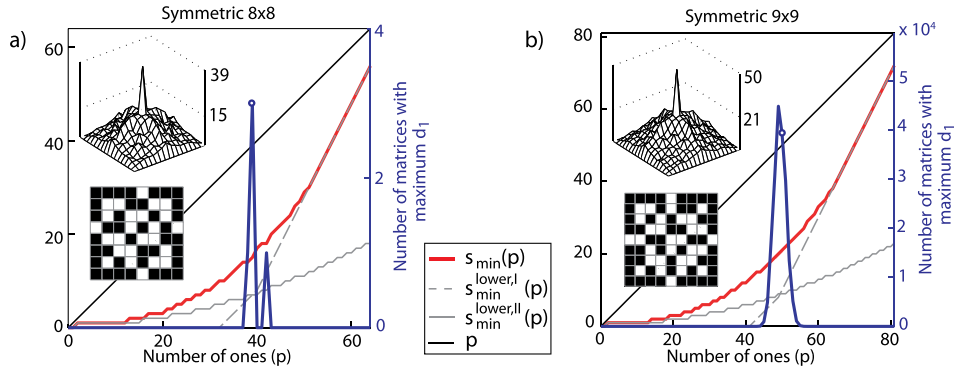

FIG. 4. (Color online) Results of the exhaustive searches for diagonally symmetric 8 × 8 and 9 × 9 matrices.

matrices for 2 × 2, 3 × 3, and 4 × 4. In Figs. 3(b), 3(c), and 3(d) we plot, in red, $s_{\min}(p)$ for matrices of sizes 5 × 5, 6 × 6, and 7 × 7. This red curve is indeed bounded from below by the gray $s_{\min}^{\text{lower,I}}(p)$ and $s_{\min}^{\text{lower,II}}(p)$ constructed in Sec. V. The number of the matrices having the maximum d_1 is plotted in blue. This curve peaks around the intersection of the $d_{1,\max}^{\text{upper,I}}$ and $d_{1,\max}^{\text{upper,II}}$ upperbounds. The circle on the blue line specifies the location of the optimal matrix ranked first by the criteria in Sec. III. The optimal matrices and their autocorrelations are shown as insets. The two numbers on the y-axes of the autocorrelation plots are the p and s values of the optimal matrices. The matrices ranked second and third and their distance spectra are listed in Appendix B.

The runtime for 7 × 7 matrices was 3 hours on 1000 Intel EM64T Nodes with 2.6 GHz clock speed. Exhaustive searches of square matrices of size 8 × 8 are not accessible to us, since the size of the search space increases exponentially with the number of matrix elements as 2^{N^2}.

VII. OBSERVATIONS ON THE OPTIMAL SQUARE MATRICES

The first interesting observation is that most top-ranked matrices in Fig. 3 are *diagonally symmetric*. Because of this if we restrict our searches to symmetric matrices of larger sizes, we still expect to find top-ranked matrices.[14] The search results for diagonally symmetric matrices of 8 × 8 and 9 × 9 are presented in Fig. 4.

The second observation for our optimal matrices shown in Fig. 3, is that d_1 always occurred in the first four neighbors of the autocorrelation peak $[A(0,\pm1), A(\pm1,0)]$. Since d_1 is the most likely point for misalignment, these matrices, although optimized for misalignment probability, also have low misalignment deviation discussed in Sec. III. Another interesting property of the autocorrelation is that the ratio of $[A(0,0) - A(\pm1,0)]/N$ or $[A(0,0) - A(0,\pm1)]/N$ is invariant under symbol expansion (i.e., expanding the number of pixels making up the original marker pixel). This property allows us to define a new quantity for the optimal matrices in this work called *sharpness* $\Lambda = d_1/N$. Since Λ is scale-invariant, d_1 can be easily obtained for different scaling factors and used to evaluate the alignment performance. The sharpness (Λ) of the optimal matrices increases with the size of the matrices.

The third observation is that all of the optimal matrices shown in Figs. 3 and 4 are connected through their black pixel (1s) and all but 3 × 3 are connected through their white pixels. A pixel is connected if one or more of its eight neighboring pixels has the same value. *Connectedness* is a preferred topological property for alignment marks; it makes the marks self-supportive, suspendible, and robust against mechanical disturbances.

The fourth observation is that the optimal matrices found in Figs. 3 and 4 are *unique*; there is only one matrix with the optimal histogram ranked by the criteria from Sec. III. In general, the mapping from histograms to correlations is not unique. For example the 2 × 2 matrices of $\begin{bmatrix} 1 & 1 \\ 0 & 0 \end{bmatrix}$ and $\begin{bmatrix} 1 & 0 \\ 0 & 1 \end{bmatrix}$ have identical histograms. It is unclear whether this property holds for optimal matrices of all sizes.

VIII. ALIGNMENT ACCURACIES OF THE OPTIMAL MATRICES

We study the performance of the optimal matrices by comparing the optimal alignment marks to the cross patterns. The matrices were embedded in a white "0" background with a size five times that of the symbol. Uniform Gaussian noise was added to all pixels to simulate a noisy image. This was correlated with its noise-free version. The alignment accuracy was determined by the deviation of the correlation peak from the center for 10 000 trials.

In Fig. 5, we plot the alignment deviation as a function of signal-to-noise ratio for two optimal marks from Fig. 3 and the crosses. The y-axis is the horizontal alignment deviation in pixels while the x-axis is the signal-to-noise ratio in decibels $[= 20\log(S/N)]$. At a signal-to-noise ratio of 0 dB, the markers are barely discernible by eye. All markers were expanded to the same area, of 35 × 35 total pixels and embedded in a background of 175 × 175 pixels, for direct comparison.

Applying the criteria from Sec. III, using the expanded 35 × 35 symbols, the 7 × 7 mark is ranked first, followed by the 5 × 5 mark, and then the crosses. The quality of the optimal alignment marks should improve with increasing size, which provides a motivation to continue the search for larger optimal matrices.

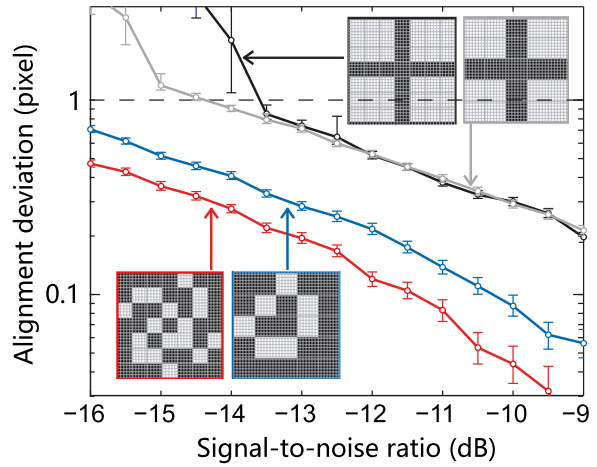

FIG. 5. (Color online) "Horizontal" alignment deviation is shown for the four alignment marks under various signal-to-noise ratios. The vertical deviation is almost identical. The color of each plot line borders the corresponding marker. All markers have been expanded to 35 × 35 pixels to illustrate the idea of pixel expansion. The top line on the right edge, corresponds to the 7 × 7 cross, while the second to top line corresponds to the 5 × 5 cross. The second to bottom line corresponds to the optimal 5 × 5 marker, while the bottom line corresponds to the optimal 7 × 7 matrix.

IX. APPLICATIONS

Correlation detection from a digital image is a simple, efficient, and reliable way to determine the position of an alignment mark. In practice, the crosscorrelations can be calculated by fast-Fourier-transforms. The peak of the correlation can further be interpolated to obtain an alignment accuracy better than the distance represented by a single pixel of the image.[9] The matrices reported in this paper are the desirable patterns to use in this context; they can replace the cross-type patterns widely in use today as position markers. Alignment using these matrices is very robust against noise in the imaging system and partial damage of the mark, providing the strongest peak signal for accurate subpixel interpolation. The potential applications of the matrices found in this paper include, but are not limited to, electron-beam lithography,[10] planar alignment in manufacturing,[15] synchronization,[16] and digital watermarking.[17]

X. CONCLUSIONS

We introduced a new class of binary matrices (two level signals) which have maximal peak-to-sidelobe distances in their aperiodic autocorrelation. Optimal square matrices of dimensions up to 7 × 7 and optimal diagonally symmetric matrices of 8 × 8 and 9 × 9 were found using a backtrack algorithm. Useful bounds, notable properties and the performances of the optimal matrices were discussed.

ACKNOWLEDGMENTS

The authors would like to thank John D. O'Brien, Robert A. Scholtz, Yuan Shen, Moe Win, Ramesh Raskar, and Steven G. Johnson for useful discussions. This work used the Extreme Science and Engineering Discovery Environment (XSEDE), which is supported by National Science Foundation grant number OCI-1053575. S.S. was supported by the MIT Undergraduate Research Opportunities program (UROP). This work was supported in part by the U.S.A.R.O. through the ISN, under Contract No. W911NF-13-D-0001. L.L. was supported in part by the MRSEC program of the NSF under Award No. DMR-1419807. L.L. and M.S. were partially supported by the MIT S3TEC Energy Research Frontier Center of the Department of Energy under Grant No. DE-SC0001299.

APPENDIX A: PROBABILITY OF MISALIGNMENT

The crosscorrelation between the data image and the reference matrix is denoted as $C(\tau_1,\tau_2)$. The autocorrelation of the binary reference matrix is denoted as $A(\tau_1,\tau_2)$. The data image is essentially a copy of the reference matrix with noise added to it. We assume the noise is Gaussian and the standard deviation for each pixel is σ. The "black" and "white" pixel values of the data image are denoted as b_i and w_i, whose expectation values are $\overline{b_i}=1$, $\overline{w_i}=0$ and $\bar{C}=A$.

Misalignment happens if $C(0,0)-C(\tau_1,\tau_2)=x_{\tau_1,\tau_2}\le 0$, representing a sidelobe $[C(\tau_1,\tau_2)]$ exceeding the central peak $[C(0,0)]$ in the crosscorrelation. Below we write this inequality in detail

$$x_{\tau_1,\tau_2}=C(0,0)-C(\tau_1,\tau_2)$$
$$=\sum_{i=1}^{p}b_i-\left\{\sum_{i=1}^{p-d_{\tau_1,\tau_2}}b_i^{(\tau_1,\tau_2)}+\sum_{i=1}^{d_{\tau_1,\tau_2}}w_i^{(\tau_1,\tau_2)}\right\}\le 0, \quad \text{(A1)}$$
$$p=A(0,0), d_{\tau_1,\tau_2}=A(0,0)-A(\tau_1,\tau_2)>0.$$

TABLE I. Peak-sidelobe distance spectra of the top-three ranked square matrices from the exhaustive search results.

N × N Ranking	d_1 n_1	d_2 n_2	d_3 n_3	d_4 n_4
3 × 3	4	5	6	7
First	4	4	12	4
Second	4	12	6	2
Third	6	6	12	0
4 × 4	7	8	9	10
First	8	8	22	10
Second	10	2	10	18
Third	12	0	8	20
5 × 5	10	11	12	13
First	4	6	10	6
Second	4	12	8	6
Third	4	12	16	12
6 × 6	14	15	16	17
First	4	16	4	2
Second	6	6	12	4
Third	6	8	12	6
7 × 7	19	20	21	22
First	14	8	6	0
Second	16	4	4	4
Third	16	4	8	4

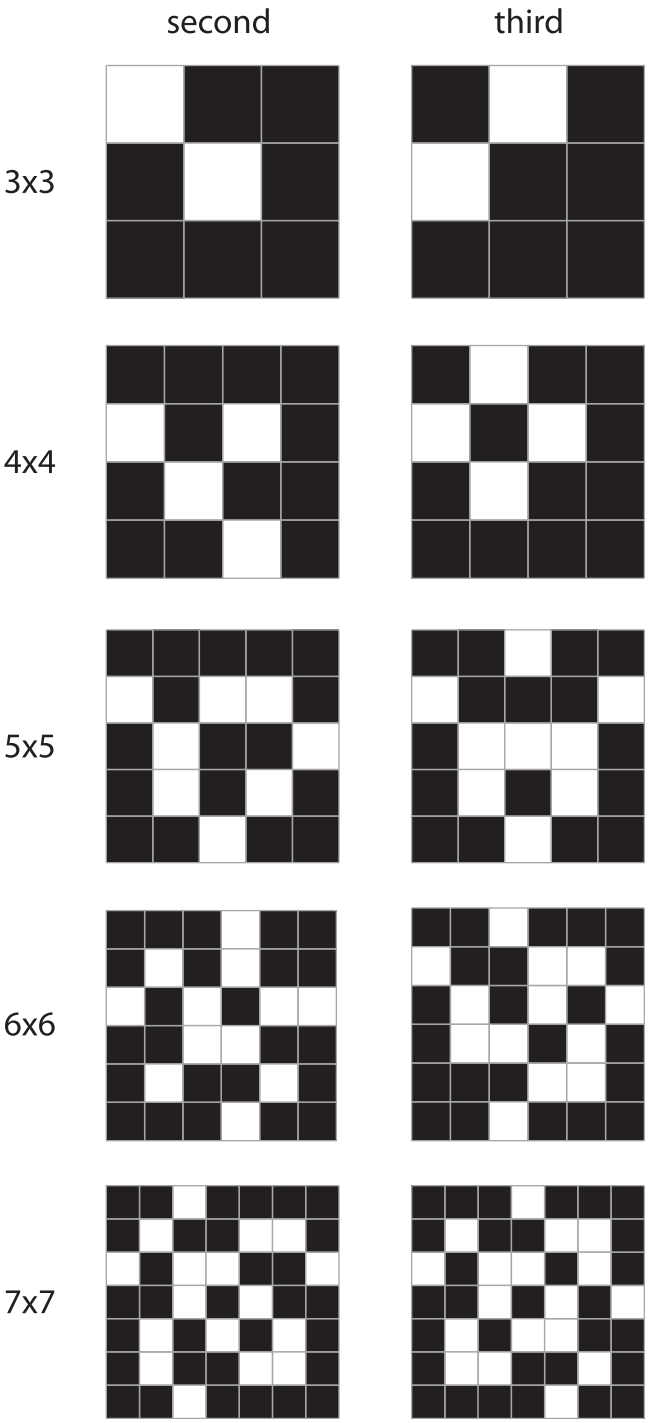

FIG. 6. Matrices ranked second and third. The first-ranked optimal matrices are shown in Fig. 3.

The first term in the inequality represents $C(0, 0)$, where each element of the reference matrix with value 1 multiplies the corresponding b_i. The sum includes all p pixels of b_i. The two terms in the brackets represent $C(\tau_1, \tau_2)$, when the reference and data matrices are offset by (τ_1, τ_2). $b_i^{(\tau_1,\tau_2)}$ is a subset of b_i which multiply elements of value 1 in the reference matrix. $w_i^{(\tau_1,\tau_2)}$ is a subset of w_i which multiply the remaining elements of value 1 in the reference matrix.

x_{τ_1,τ_2} is a sum of Gaussian variables and so is also a Gaussian variable with an expectation value $\overline{x_{\tau_1,\tau_2}} = d_{\tau_1,\tau_2}$. By bookkeeping the terms in Eq. (A1), one finds the standard deviation $\sigma^2_{x_{\tau_1,\tau_2}} = 2d_{\tau_1,\tau_2}\sigma^2$.

The probability of misalignment due to the sidelobe at (τ_1, τ_2) is $M(x_{\tau_1,\tau_2} \le 0)$

$$M\left(x_{\tau_1,\tau_2} \le 0 | \overline{x_{\tau_1,\tau_2}} = d_{\tau_1,\tau_2}\right) = \int_{-\infty}^{0} \frac{1}{\sqrt{2\pi}\sigma_{x_{\tau_1,\tau_2}}} \exp\left[\frac{-(x_{\tau_1,\tau_2} - d_{\tau_1,\tau_2})^2}{2\sigma^2_{x_{\tau_1,\tau_2}}}\right] dx_{\tau_1,\tau_2} = \frac{1}{2}\mathrm{Erfc}\left(\frac{\sqrt{d_{\tau_1,\tau_2}}}{2\sigma}\right) = M\left(\frac{d_{\tau_1,\tau_2}}{\sigma^2}\right).$$

Here, the complementary error function is $\mathrm{Erfc}(t) = (2/\sqrt{\pi}) \int_t^\infty dt' \exp(-t'^2)$.

The probability of misalignment (PoM) is the union of the probability in the spaces bounded by all the inequalities $(x_{\tau_1,\tau_2} \le 0)$ at sidelobe positions $(\tau_1, \tau_2 \ne 0, 0)$. The individual spaces bounded by the inequalities overlap in general making the exact calculation of PoM difficult. However, it is easy to find an upper bound for the PoM by assuming no overlap between these spaces. Specifically, $PoM \le \sum_{(\tau_1,\tau_2\ne 0,0)} M(x_{\tau_1,\tau_2} \le 0)$ (Ref. 2) where the sum is over all sidelobes.

$M(d_{\tau_1,\tau_2}/\sigma^2)$ decreases as the distance d_{τ_1,τ_2} increases. Consequently, a good criterion should tend to maximize the overall d_i in order to minimize the probability of misalignment. Also, it is of higher priority to maximize the smaller distance, which contributes more to the PoM. This is the basis of our ranking criteria, which is completely justified in the low noise limit. Under the low noise limit, the terms of larger d_i make vanishingly small contributions compared to the term of smaller d_i. We show this in Eq. (A2) by noticing that Erfc (t) can be approximated by $(2/\sqrt{\pi})[\exp(-t^2)/t]$ for large t (or small σ).

$$\lim_{\sigma\to 0} \frac{M\left(d_{i+1}/\sigma^2\right)}{M\left(d_i/\sigma^2\right)} = \lim_{\sigma\to 0} \exp\left[-\frac{d_{i+1} - d_i}{2\sigma^2}\right] \frac{\sqrt{d_i}}{\sqrt{d_{i+1}}} = 0. \tag{A2}$$

However, the ranking criteria, in general, depend on the noise level σ. We note, due to the central limit theorem, the above results still hold for non-Gaussian noise distributions, when the matrix size is large.

APPENDIX B: DISTANCE SPECTRA

In order to provide additional useful matrices and to illustrate our ranking criteria, we tabulated, in Table I, part of the peak-sidelobe distance spectra for the top-three ranked square matrices from the exhaustive search results. The values of the first four distances (d_1, d_2, d_3, and d_4) and the numbers (n_1, n_2, n_3, and n_4) of the corresponding sidelobes are listed. Those top-three binary square matrices are shown in Figs. 3 and 6.

[1]R. H. Barker, *Communications Theory* (Butterworth, London, 1953), p. 273.
[2]F. Neuman and L. Hofman, IEEE Aerosp. Electron. Syst. Mag. **3**, 570 (1971).

[3]S. W. Golomb and G. Gong, *Signal Design for Good Correlation: For Wireless Communication, Cryptography, and Radar* (Cambridge University, New York, 2004).
[4]S. R. Gottesman and E. E. Fenimore, Appl. Opt. **28**, 4344 (1989).
[5]S. Alquaddoomi and R. Scholtz, IEEE Trans. Inf. Theory **35**, 1048 (1989).
[6]J. Costas, Proc. IEEE **72**, 996 (1984).
[7]S. Golomb and H. Taylor, IEEE Trans. Inf. Theory **28**, 600 (1982).
[8]G. Ramakrishna and W. Mow, *Sequences and Their Applications—SETA 2004* (Springer, New York, 2005), Vol. 3486, p. 71.
[9]E. H. Anderson, D. Ha, and J. A. Liddle, Microelectron. Eng. **73**, 74 (2004).
[10]V. Boegli and D. P. Kern, J. Vac. Sci. Technol., B **8**, 1994 (1990).
[11]M. Qi, E. Lidorikis, P. T. Rakich, S. G. Johnson, J. D. Joannopoulos, E. P. Ippen, and H. I. Smith, Nature **429**, 538 (2004).
[12]L. Lu, "Photonic crystal nanocavity lasers for integration," Ph.D. thesis (University of Southern California, 2010).
[13]J. Robinson, IEEE Trans. Inf. Theory **43**, 290 (1997).
[14]J. Shearer, IEEE Trans. Inf. Theory **50**, 1846 (2004).
[15]H. Sakou, T. Miyatake, S. Kashioka, and M. Ejiri, IEEE Trans. Acoust. Speech Signal Process. **37**, 2148 (1989).
[16]R. Scholtz, IEEE Trans. Comm. **28**, 1204 (1980).
[17]A. Tirkel, C. Osborne, and T. Hall, Signal Process. **66**, 373 (1998).